On the Use of Multiple Measurement Models for Extended Target Tracking

Karl Granström and Christian Lundquist
Department of Electrical Engineering, Linköping University, Linköping, Sweden
Email: karl@isy.liu.se and lundquist@isy.liu.se

***Abstract*—This paper considers extended targets that have constant extension shapes, but generate measurements whose appearance can change abruptly. The problem is approached using multiple measurement models, where each model corresponds to a measurement appearance mode. Mode transitions are modeled as dependent on the extended target kinematic state, and a multiple model extended target PHD filter is used to handle multiple targets with multiple appearance modes. The extended target tracking is evaluated using real world data where a laser range sensor is used to track multiple bicycles.**

I. Introduction

Multiple target tracking can be defined as the processing of multiple measurements obtained from multiple targets in order to maintain estimates of the targets' current states, see e.g. [1]. In this context an extended target is defined as a target that potentially gives rise to more than one measurement per time step.

In extended target tracking measurement modeling is of high importance. Part of the measurement modeling is to model the target's extension, i.e. the shape and the size of the target. The extension parameters are estimated using the multiple measurements, and subsequently the appearance of the measurements in the measurement space is important both for the choice of shape model, and for the modeling of how the measurements relate to the shape parameters. For example an extended target with a rectangular extension will, if measured by a laser range sensor, give rise to measurements whose appearance is either line-shaped or L-shaped [2].

In this paper we consider tracking of extended targets with a constant shape and an appearance in the measurement space that can change significantly with the sensor to target geometry. Specifically we are concerned with targets whose measurement appearance changes abruptly, and we do not consider targets whose appearance changes slowly w.r.t. sample time. Thus while the target shape is constant, there are several measurement appearance modes between which the target switches. Depending on the appearance mode, the different state variables may or may not be observable. The different ways to model this type of extended target tracking scenario are here divided into three complexity levels:

1: The most advanced approach is to construct a measurement model that is capable of handling a broad variety of both different shapes and different measurement appearances. While such a model would be most general, it could also prove to be overly computationally complex.

2: A simpler level of modeling is to assume a specific geometric shape for the target, such as an ellipse, a line or a rectangle. The measurement model must then include a capability of distinguishing which appearance mode the current measurements are in.

3: The simplest level of modeling is to not model the shape at all, i.e. to only estimate the target's kinematic properties. This approach has lowest computational complexity and the flexibility to track different type of targets is high because this model, even though it is simplistic in terms of target shape, is applicable (with varying degree of accuracy) to all of the appearance modes.

In this paper the problem of extended target tracking under multiple appearance modes is given a practical context by considering bicycle tracking using a laser range sensor. The shape of a bicycle does not change over time, and from a bird's-eye view the shape can be approximated as a thin stick. Under an assumed stick shape, for each appearance mode the measurement model, according to level 2 above, must describe how the measurements relate to the position, the orientation and the length of the stick.

Fig. 1 shows three examples of laser range measurements caused by a bicycle. From the data in Fig. 1a the position, orientation and length of a stick target is observable. In comparison, the data in Fig. 1c is more suitable for a target modeled without a shape (level 3 above), since the length is not observable from this type of data, and the orientation can only be observed using a sequence of measurement sets under the assumption that the orientation and the target's heading coincides. The data in Fig. 1b resides somewhere in between the stick model and the point model: it is difficult to determine which is the most appropriate model. r Due to the difficulty of deciding which appearance mode that laser range data is in, in this paper we do not construct a single measurement model that incorporates a measurement mode decision. Instead we use multiple measurement models that correspond to the multiple appearance modes. For bicycles measured by a laser sensor a stick shape is assumed and two measurement models are used: one line model that corresponds to Fig. 1a and one point model that corresponds to Fig. 1c. The multiple measurement models are used together with multiple motion models in a multiple model (MM) framework, a model for state dependent mode transitions is suggested, and multiple stick shaped extended targets are handled with a MM extended target probability hypothesis density (MM-ET-PHD) filter.

The paper is outlined as follows: Related work is described in Section II, the MM-ET-PHD filter is described in Section III, the multiple models are given in Section IV, results are presented in Section V and Section VI concludes the paper.

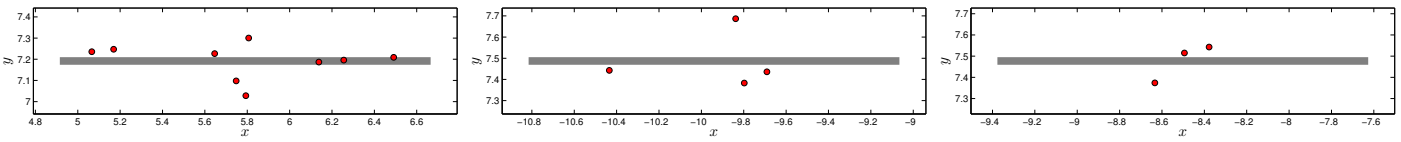

(a) (b) (c)

Fig. 1. Real world data examples from bicycle tracking using a laser range sensor, the target shape is modeled as a thin stick (gray). (a) The measurements (red) are spread along the entire length of the target. (b) The measurements are spread in a way that makes it difficult to say whether or not they were caused by the center of the target, or its entire length. (c) The measurements are spread around the center of the target. An extended target measurement model must be able to handle both ambiguous cases (e.g. (b)) and unambiguous cases (e.g. (a) and (c)).

II. Related work

Spatial distribution models in extended target tracking appeared in [3], [4]. Under this model each extended target measurement is a random sample of a distribution that is dependent on the extended target state. A number of different extended target measurement models have been presented, where the targets are modeled as sticks [4]–[6], circles [7], ellipses [2], [8]–[14], rectangles [2], or general shapes [15], [16].

To use multiple models, in the literature also called jump Markov system models, have proven to be a powerful way to model target tracking. The interactive multiple model IMM algorithm [17] represents a good trade-off between computational complexity and tracking performance, and has been shown to perform well for maneuvering single point target tracking. Multiple models have been used in extended target tracking for different types of motion [13], [18]. Multiple measurement models were used for elliptical and rectangular extended targets in [2], however it was assumed that a target cannot transition between different shapes and therefore a MM framework was not necessary.

Finite set statistics (FISST) [19] represents a rigorous approach to multiple target tracking. It has led to the point target probability hypothesis density (PHD) filter [20], with its Gaussian mixture (GM) implementation [21]. An extension of the PHD filter to handle extended targets of the type presented in [3] is given in [22], with implementations in [23]–[25]. An overview of MM-PHD filters is given in [26], and [27] is pointed out as the preferred MM-PHD approach.

TABLE I. Notation

- $\mathbb{R}^n$ is the set of real n-vectors, $\mathbb{S}_+^n$ is the set of symmetric positive semi-definite $n \times n$-matrices, and $\mathbb{N}_+$ is the set of natural numbers.
- At discrete time t_k, $\mathbf{x}_k \in \mathbb{R}^{n_x}$ is the extended target kinematic state, $o_k \in M \subset \mathbb{N}_+$ is the extended target mode, and $\xi_k = (\mathbf{x}_k\ ,\ o_k) \in \mathcal{X}_0 = \mathbb{R}^{n_x} \times M$ is the augmented extended target state.
- $\mathcal{N}(x\,;\,m,P)$ denotes the probability density function (pdf) of a Gaussian distribution defined over the vector x, with mean vector $m \in \mathbb{R}^n$ and covariance matrix $P \in \mathbb{S}_+^n$. The short hand notation $\mathcal{N}(x,\Theta)$ is also used, where $\Theta = (m,P)$.
- $\mathbf{Z}_k = \left\{\mathbf{z}_k^{(j)}\right\}_{j=1}^{N_{z,k}}$ is a measurement set at time t_k, where $\mathbf{z}_k^{(j)} \in \mathbb{R}^{n_z}$, $\forall j$.
- $\mathrm{p} \angle \mathbf{Z}$ denotes all the partitions p of the set $\mathbf{Z}$. A partition p is a set of non-empty subsets W called cells. The union of all cells W is equal to the set $\mathbf{Z}$. The cardinality of a cell W is denoted $|W|$.
- $\delta_{i,j}$ is the Kronecker delta, and $\otimes$ is the Kronecker product.
- $f[g(x)]$ denotes the integral $\int f(x)g(x)dx$.
- $\mathrm{sinc}(t) = \sin(t)/t$ is the sinc function.
- $\mathbf{I}_n$ is a $n \times n$ identity matrix and $\mathbf{0}_n$ is a $n \times n$ all zero matrix..

III. MM-ET-PHD

In this section we describe a MM extended target PHD filter (MM-ET-PHD). The filter is an adaptation of the GM implementation [23], [24] of the extended target PHD filter [22] into the MM framework in [26], [27]. Due to space constraints derivations are omitted. Notation is presented in Table I.

Given a predicted PHD $D_{k|k-1}(\xi)$ and a set of measurements $\mathbf{Z}_k$ the posterior PHD is [22]

$$D_{k|k}(\xi) = L_{\mathbf{Z}}(\xi) D_{k|k-1}(\xi), \tag{1a}$$

$$\begin{aligned} L_{\mathbf{Z}}(\xi) = &\left(1 - e^{-\gamma(\xi)}\right) P_D(\xi) + e^{-\gamma(\xi)} P_D(\xi) \\ &\times \sum_{\mathrm{p} \angle \mathbf{Z}_k} \omega_{\mathrm{p}} \sum_{W \in \mathrm{p}} \frac{\gamma(\xi)^{|W|}}{d_W} \prod_{\mathbf{z}_k \in W} \frac{\varphi_{\mathbf{z}_k}(\xi)}{\lambda_k c_k(\mathbf{z}_k)}, \end{aligned} \tag{1b}$$

$$\omega_{\mathrm{p}} = \frac{\prod_{W \in \mathrm{p}} d_W}{\sum_{\mathrm{p}' \angle \mathbf{Z}_k} \prod_{W' \in \mathrm{p}'} d_{W'}}, \tag{1c}$$

$$\begin{aligned} d_W = &\delta_{|W|,1} \\ &+ D_{k|k-1} \left[P_D(\xi) \gamma(\xi)^{|W|} e^{-\gamma(\xi)} \prod_{\mathbf{z}_k \in W} \frac{\varphi_{\mathbf{z}_k}(\xi)}{\lambda_k c_k(\mathbf{z}_k)} \right], \end{aligned} \tag{1d}$$

where $P_D(\xi)$ is the probability of detection, $\gamma(\xi)$ is the measurement rate, $\varphi_{\mathbf{z}_k}(\xi)$ is the likelihood function for a single target generated measurement, and $\lambda_k c_k(\mathbf{z}_k)$ is the clutter likelihood. The measurements are modeled using a state space model

$$\mathbf{z}_k = h_k(\xi_k) + \mathbf{e}_k, \tag{2}$$

where $\mathbf{e}_k$ is zero mean Gaussian measurement noise, and the measurement model $h(\,\cdot\,) : \mathcal{X}_0 \to \mathbb{R}^{n_z}$ is generally non-linear.

Given a posterior PHD $D_{k|k}(\xi)$ the predicted PHD is [19]

$$D_{k+1|k}(\xi) = D_k^b(\xi) + \int P_S(\xi') p(\xi|\xi') D_{k|k}(\xi') \mathrm{d}\xi', \tag{3}$$

where $D_k^b(\xi)$ is the birth PHD, $P_S(\xi)$ is the probability of target survival, and target spawning has been omitted for the sake of simplicity, see [28] for work on extended target spawning. The single target transition density $p(\xi_{k+1}|\xi_k)$ describes the time evolution of the extended target state from time t_k to time t_{k+1}. The transition density can be decomposed as follows

$$\begin{aligned} p(\xi_{k+1}|\xi_k) &= p(\mathbf{x}_{k+1}|o_{k+1}, \mathbf{x}_k, o_k)\, p(o_{k+1}|\mathbf{x}_k, o_k) && \text{(4a)} \\ &= p(\mathbf{x}_{k+1}|o_{k+1}, \mathbf{x}_k)\, p(o_{k+1}|\mathbf{x}_k, o_k), && \text{(4b)} \end{aligned}$$

where the second equality follows from a standard Markov-type assumption. In much previous MM target tracking, see

e.g. [27], [29], it is assumed that the mode transition density is independent of the kinematic state, i.e. it is assumed that $p\left(o_{k+1}\left|\mathbf{x}_k, o_k\right.\right) = p\left(o_{k+1}\left|o_k\right.\right)$.

This assumption holds when the different modes correspond to different types of kinematic motion, e.g. probability of a switch from CT motion to CV motion can reasonably be seen as independent of the target kinematics. However, as will be illustrated in Section IV, the assumption does not necessarily hold when the modes also correspond to different measurement models. Therefore the assumption $p\left(o_{k+1}\left|\mathbf{x}_k, o_k\right.\right) = p\left(o_{k+1}\left|o_k\right.\right)$ is relaxed in this paper. The mode transition probabilities are organized in a transition probability matrix $T_{k+1|k}\left(\mathbf{x}_k\right)$, where the ith row and jth column correspond to $p\left(o_{k+1} = j\left|\mathbf{x}_k, o_k = i\right.\right)$.

The time evolution of the target kinematics is described by a state space motion model

$$\mathbf{x}_{k+1} = f_k\left(\mathbf{x}_k,\ o_{k+1}\right) + \mathbf{w}_{k+1}, \tag{5}$$

where $\mathbf{w}_k$ is zero mean Gaussian process noise. The motion model $f(\cdot) : \mathcal{X}_0 \to \mathbb{R}^{n_x}$ is generally non-linear, a thorough overview of state transition functions is given in [30].

Assumptions are listed in Section III-A and the correction and prediction are given in Section III-B and Section III-C, respectively. Complexity reduction of the MM-ET-PHD filter is discussed in Section III-D.

A. Assumptions

Assumption 1: The probability of detection, the probability of survival and the measurement rate are constant, i.e.,

$$P_{D,k}\left(\xi\right) = P_D,\ P_{S,k}\left(\xi\right) = P_S,\ \gamma\left(\xi\right) = \gamma. \tag{6}$$

These assumptions are not immediately necessary to obtain an MM-ET-PHD filter, in this paper they are made for the sake of simplicity. □

Assumption 2: For the mode transition density,

$$\begin{aligned} p\left(o_{k+1}|\mathbf{x}_k, o_k\right)&\mathcal{N}\left(\mathbf{x}_k\ ;\ \Theta^{(j)}_{k|k}(o_k)\right) \\ \approx& p\left(o_{k+1}\left|m^{(j)}_{k|k}(o_k), o_k\right.\right)\mathcal{N}\left(\mathbf{x}_k\ ;\ \Theta^{(j)}_{k|k}(o_k)\right) \end{aligned} \tag{7}$$

is assumed to hold for all components j. The transition density is abbreviated as $p^{(j)}_{k+1|k}\left(o|o'\right) = p\left(o_{k+1}|m^{(j)}_{k|k}(o_k), o_k\right)$. Trivially this assumption holds if the mode transition is independent of the kinematic state. In general assumption 2 holds when the transition density does not vary much in the uncertainty zone of the kinematic state space, determined by $P^{(j)}_{k|k}(o_k)$. This is true either when $p\left(o_{k+1}|\mathbf{x}_k, o_k\right)$ is a sufficiently smooth function w.r.t $\mathbf{x}_k$, or when the uncertainty zone is sufficiently small. □

Assumption 3: Similarly to previous distribution mixture implementations of the PHD filter, see e.g. [21], [23]–[25], the birth PHD is assumed to be a GM,

$$D^b_k\left(\xi\right) = \pi_k\left(o\right)\sum_{j=1}^{J_k(o)} w^{(j)}_{b,k}\left(o\right)\mathcal{N}\left(\mathbf{x}\ ;\ \Theta^{(j)}_{b,k}\left(o\right)\right). \tag{8}$$

The specific form used here was given in [27]. □

B. Correction

If the predicted PHD has the following GM representation

$$D_{k|k-1}\left(\xi\right) = \sum_{j=1}^{J_{k|k-1}(o)} w^{(j)}_{k|k-1}\left(o\right)\mathcal{N}\left(\mathbf{x}\ ;\ \Theta^{(j)}_{k|k-1}\left(o\right)\right), \tag{9}$$

the posterior intensity has the following GM representation

$$\begin{aligned} D_{k|k}\left(\xi\right) =& \left(1 - P_D\right)D_{k|k-1}\left(\xi\right) \\ &+ \sum_{\mathrm{p}\angle\mathbf{Z}_k}\sum_{W\in\mathrm{p}} D^z_{k|k-1}\left(\xi, W\right) \end{aligned} \tag{10a}$$

$$D^z_{k|k-1}\left(\xi, W\right) = \sum_{j=1}^{J_{k|k-1}(o)} w^{W,(j)}_{k|k}\left(o\right)\mathcal{N}\left(\mathbf{x}\ ;\ \Theta^{W,(j)}_{k|k}\left(o\right)\right). \tag{10b}$$

Measurement set partitions p are obtained using the Distance Partition algorithm from [23], [24]. The corrected Gaussian parameters are

$$\Theta^{W,(j)}_{k|k}\left(o\right) = \left(m^{W,(j)}_{k|k}\left(o\right)\ ,\ P^{W,(j)}_{k|k}\left(o\right)\right) \tag{11a}$$

$$m^{W,(j)}_{k|k}\left(o\right) = m^{(j)}_{k|k-1}\left(o\right) + K^{W,(j)}_k(o)\varepsilon^{(j)}_W(o) \tag{11b}$$

$$P^{W,(j)}_{k|k}\left(o\right) = \left(\mathbf{I} - K^{W,(j)}_k(o)H^{(j)}_k(o)\right)P^{(j)}_{k|k-1}(o) \tag{11c}$$

$$\varepsilon^{(j)}_W(o) = \mathbf{z}_W - \hat{\mathbf{z}}^{(j)}_W(o) \tag{11d}$$

$$S^{W,(j)}_k(o) = H^{(j)}_k(o)P^{(j)}_{k|k-1}(o)\left(H^{(j)}_k(o)\right)^{\mathrm{T}} + R_k(o) \tag{11e}$$

$$K^{W,(j)}_k(o) = P^{(j)}_{k|k-1}(o)\left(H^{(j)}_k(o)\right)^{\mathrm{T}}\left(S^{W,(j)}_k(o)\right)^{-1} \tag{11f}$$

where $\mathbf{z}_W$ is a vertical vectorial concatenation of the measurements in the cell, $\hat{\mathbf{z}}^{(j)}_W(o)$ is the corresponding predicted measurement and $H^{(j)}_k(o)$ is the Jacobian of $\hat{\mathbf{z}}^{(j)}_W(o)$ w.r.t. $\mathbf{x}_k$, evaluated at $m^{(j)}_{k|k-1}(o)$. The corrected weights are

$$w^{W,(j)}_{k|k}\left(o\right) = \frac{\omega_{\mathrm{p}}}{d_W}\Gamma_W\Phi^{(j)}_W(o)w^{(j)}_{k|k-1}(o), \tag{12a}$$

$$\Gamma_W = e^{-\gamma}\gamma^{|W|}P_D \tag{12b}$$

$$\Phi^{(j)}_W(o) = \varphi^{(j)}_W(o)\prod_{\mathbf{z}_k\in W}\frac{1}{\lambda_k c_k\left(\mathbf{z}_k\right)} \tag{12c}$$

$$d_W = \delta_{|W|,1} + \sum_{o}\sum_{\ell=1}^{J_{k|k-1}(o)}\Gamma_W\Phi^{(\ell)}_W(o)w^{(\ell)}_{k|k-1}(o) \tag{12d}$$

where ω_{p} is given in (1c) and $\varphi^{(j)}_W\left(o\right)$ is the measurement likelihood of W w.r.t. the jth component.

C. Prediction

If the posterior PHD has the following GM representation

$$D_{k|k}\left(\xi\right) = \sum_{j=1}^{J_{k|k}(o)} w^{(j)}_{k|k}\left(o\right)\mathcal{N}\left(\mathbf{x}\ ;\ \Theta^{(j)}_{k|k}\left(o\right)\right), \tag{13}$$

the predicted PHD has the following GM representation [27]

$$D_{k+1|k}\left(\xi\right) = D^b_k\left(\xi\right) + D^f_{k+1|k}\left(\xi\right). \tag{14}$$

The birth PHD was given in assumption 3, and the prediction of existing targets is a GM

$$D^{f}_{k+1|k}(\xi) = \sum_{o'}\sum_{j=1}^{J_{k|k}(o')} w^{(j)}_{k+1|k}(o,o')\,\mathcal{N}\left(\mathbf{x}\,;\ \Theta^{(j)}_{k+1|k}(o,o')\right) \tag{15a}$$

$$w^{(j)}_{k+1|k}(o,o') = P_S p^{(j)}_{k+1|k}(o|o')\, w^{(j)}_{k|k}(o') \tag{15b}$$

$$\Theta^{(j)}_{k+1|k}(o,o') = \left(m^{(j)}_{k+1|k}(o,o')\ ,\ P^{(j)}_{k+1|k}(o,o')\right) \tag{15c}$$

$$m^{(j)}_{k+1|k}(o,o') = f_k\left(m^{(j)}_{k|k}(o'),o\right) \tag{15d}$$

$$P^{(j)}_{k+1|k}(o,o') = F^{(j)}_{k}(o)\,P^{(j)}_{k|k}(o')\left(F^{(j)}_{k}(o)\right)^{\mathrm{T}} + Q_{k+1}(o)\,. \tag{15e}$$

where $p^{(j)}_{k+1|k}(o|o')$ is the transition probability computed under Assumption 2, and $F^{(j)}_{k}(o)$ is the Jacobian of $f_k(\cdot)$ w.r.t. $\mathbf{x}_k$, evaluated at $m^{(j)}_{k|k}(o')$.

D. Complexity reduction

Just as in the other distribution mixture implementations of the PHD filter [21], [23]–[25], [27], the number of components in the PHD intensity increases after prediction and correction. This problem can be alleviated by using mixture reduction procedures, like pruning and merging. In this paper, after each PHD correction, components with weight $w^{(j)}_{k|k}(o) < \tau$ are pruned. After pruning, components are merged using a merging algorithm similar to the one suggested in [21, Table II]. The Kullback-Leibler difference, see e.g. [31, Equation (17)], is used as merging criterion. Merging is only performed within the modes, i.e. Gaussian components are not merged if they have different modes.

IV. Multiple Model Framework for Bicycle Tracking Using Laser Data

In this section we describe the multiple models that are used for bicycle tracking using laser data. The kinematic state vector $\mathbf{x}_k$ is chosen to be

$$\mathbf{x}_k = [\mathsf{x}_k,\ \mathsf{y}_k,\ \mathsf{v}_k,\ \phi_k,\ \omega_k]^{\mathrm{T}}, \tag{16}$$

where $(\mathsf{x}_k, \mathsf{y}_k)$ is the position in Cartesian coordinates, v_k is the speed, ϕ_k is the heading and ω_k is the turn-rate. For sake of simplicity it is assumed that all bicycles are of equal length ℓ, and it is assumed that target's heading and the stick's orientation coincides. It is straightforward to adapt the models below to allow for estimation of the bike length. Mode transitions are described in Section IV-A, and two different types of motion modes are considered in Section IV-B. Motion along a fixed heading at constant speed can be described by a constant velocity model (CV) and a turn can be described by a coordinated turn model (CT). Furthermore two different types of measurement models, a point (P) and a line (L) model, are used to describe the relation between the measurements and the state variable, see Section IV-C. This gives four different modes in total (i.e. $M = \{1,2,3,4\}$):

1) CT motion, P measurements (CTP),
2) CV motion, P measurements (CVP),
3) CT motion, L measurements (CTL),
4) CV motion, L measurements (CVL).

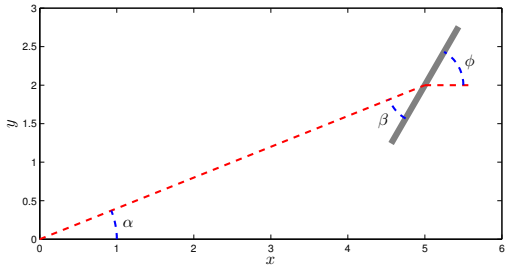

Fig. 2. Illustration of sensor to target geometry. The stick target (gray) has center position $(\mathsf{x},\mathsf{y}) = (5,2)$ and heading ϕ. The point mode is most likely when $\cos(\beta) \approx \pm 1$, and the line mode is most likely when $\cos(\beta) \approx 0$.

A. Mode transitions

The modes follow a discrete Markov chain, where the transition probability matrix is decomposed as follows

$$T_{k+1|k}(\mathbf{x}_k) = T^{\text{Meas}}_{k+1|k}(\mathbf{x}_k) \otimes T^{\text{Motion}}_{k+1|k}. \tag{17}$$

The transitions between CT and CV motion are modeled as independent of the kinematic state, something that holds in most cases. The probability of staying in the same motion mode is here given by P_{same}, which gives the following transition probability matrix for the motion modes,

$$T^{\text{Motion}}_{k+1|k} = \begin{bmatrix} P_{\text{same}} & 1-P_{\text{same}} \\ 1-P_{\text{same}} & P_{\text{same}} \end{bmatrix}. \tag{18}$$

In this paper, the transitions between P and L measurement modes are modeled as dependent on the kinematic state. The transition probability matrix for the measurement modes is

$$T^{\text{Meas}}_{k+1|k}(\mathbf{x}_k) = \begin{bmatrix} P_{\text{point}}(\mathbf{x}_k) & 1-P_{\text{point}}(\mathbf{x}_k) \\ P_{\text{point}}(\mathbf{x}_k) & 1-P_{\text{point}}(\mathbf{x}_k) \end{bmatrix}, \tag{19}$$

where the probability of transition to, or staying in, the point measurement mode is given by a kinematic state dependent probability $P_{\text{point}}(\mathbf{x}_k)$.

The intuition behind this model is illustrated in Fig. 2. If $\cos(\beta) \approx \pm 1$ then the bicycle's heading is lined up with the sensor, and in this case the probability that the bicycle will generate point measurements in the next time-step is larger. If $\cos(\beta) \approx 0$ the bicycle is perpendicular to the vector from the sensor to the center point, in which case the probability that the bicycle will generate point measurements in the next time-step is smaller. Thus, the probability of transition to, or staying in, the point mode can be seen as a function of $\cos(\beta)$. With simple trigonometry it is easy to show $\beta = \phi - \alpha$, which clearly is a function of the kinematic state $\mathbf{x}$. Specifically we use the following model for $P_{\text{point}}(\mathbf{x}_k)$,

$$P_{\text{point}}(\mathbf{x}_k) = \frac{1 + (1-2P_{\text{min}})\cos\left(2\left(\phi_k - \alpha_k\right)\right)}{2} \tag{20}$$

where α_k is the angle from the sensor to the Cartesian position $(\mathsf{x}_k, \mathsf{y}_k)$, and $P_{\text{min}} \in (0\ ,\ 0.5)$ is used to ensure that $P_{\text{point}}(\mathbf{x}_k) \in [P_{\text{min}}\ ,\ 1-P_{\text{min}}]$.

B. Kinematic state motion models

The time evolution of the kinematic state is modeled as

$$\begin{aligned} &p\left(\mathbf{x}_{k+1}\,|o_{k+1},\mathbf{x}_k\right) \\ &\quad = \mathcal{N}\left(\mathbf{x}_{k+1}\,;\ f_k\left(\mathbf{x}_k,o_{k+1}\right), Q_{k+1}(o_{k+1})\right). \end{aligned} \tag{21}$$

For the four modes listed above we have $f_k(\mathbf{x}_k, o_{k+1}=1,3) = f_{\text{CT}}(\mathbf{x}_k)$ and $f_k(\mathbf{x}_k, o_{k+1}=2,4) = f_{\text{CV}}(\mathbf{x}_k)$. A constant turn-rate motion model for the state vector (16) is [30, Eq. (75)]

$$f_{\text{CT}}(\mathbf{x}_k) = \begin{bmatrix} \mathsf{x}_k + T\mathsf{v}_k \operatorname{sinc}\left(\frac{T\omega_k}{2}\right)\cos\left(\phi_k + \frac{T\omega_k}{2}\right) \\ \mathsf{y}_k + T\mathsf{v}_k \operatorname{sinc}\left(\frac{T\omega_k}{2}\right)\sin\left(\phi_k + \frac{T\omega_k}{2}\right) \\ \mathsf{v}_k \\ \phi_k + T\omega_k \\ \omega_k \end{bmatrix} \tag{22}$$

At a turn-rate of zero the coordinated turn model can be reduced to the following constant velocity motion model,

$$f_{\text{CV}}(\mathbf{x}_k) = \begin{bmatrix} \mathsf{x}_k + T\mathsf{v}_k\cos(\phi_k) \\ \mathsf{y}_k + T\mathsf{v}_k\sin(\phi_k) \\ \mathsf{v}_k \\ \phi_k \\ 0 \end{bmatrix}. \tag{23}$$

Here the turn-rate ω_k is set to zero, a procedure that avoids having kinematic state vectors with unequal dimensions for the different motion modes. State vectors with unequal dimensions may cause problems, e.g. the mixing step of the IMM algorithm suffers from a bias when the modes have state vectors with unequal dimension, a problems which is solved in [32]. Since there is no mixing in the MM-ET-PHD filter it does not suffer from this bias. It remains within future work to investigate if the motion model (23) can be improved.

The process noise covariance matrix is [30, Equation (76)]

$$Q_k(o_k) = \text{blkdiag}\left(\mathbf{0}_2\ ,\ T^2\sigma_v^2\ ,\ \begin{bmatrix} T^3\sigma_\omega^2/3 & T^2\sigma_\omega^2/2 \\ T^2\sigma_\omega^2/2 & T^2\sigma_\omega^2 \end{bmatrix}\right). \tag{24}$$

C. Measurement models

This section describes two measurement likelihood models

$$\prod_{\mathbf{z}_k\in W}\varphi_{\mathbf{z}_k}(\xi) = p(W|\xi) \tag{25}$$

that are applicable to bicycle tracking using laser range sensors.

1) Point measurement model: The point measurement model corresponds to when the bicycle is lined up with the measurement bearing, i.e. either the front or the rear wheel is pointing approximately directly at the sensor. This corresponds to $\cos(\beta) \approx \pm 1$ in Fig. 2. In this case measurements are typically caused by the feet of the rider. Because the pedals are located close to the lengthwise middle point of a bicycle, in the point measurement model the likelihood is modeled as follows,

$$p(W|\mathbf{x}, o=1,2) = \prod_{j=1}^{|W|}\mathcal{N}\left(\mathbf{z}^{(j)}\,;\, H\mathbf{x}, \sigma_P^2\mathbf{I}_2\right) \tag{26a}$$

$$H = \begin{bmatrix} 1 & 0 & 0 & 0 & 0 \\ 0 & 1 & 0 & 0 & 0 \end{bmatrix} \tag{26b}$$

The product of Gaussians can be rewritten as

$$p(W|\mathbf{x}, o=1,2) = \mathcal{N}\left(\mathbf{z}_W\,;\,\mathbf{H}_W\mathbf{x}, \sigma_P^2\mathbf{I}_{2|W|}\right), \tag{27}$$
$$\mathbf{H}_W = [\underbrace{H^{\text{T}}, \cdots, H^{\text{T}}}_{|W| \text{ times}}]^{\text{T}}.$$

TABLE II. LINE MEASUREMENT MODEL ASSOCIATION

1: **Input:** Cell W, set of MGPs and kinematic estimate $\hat{\mathbf{x}}$
2: Transform measurements in cell using function outlined below.
3: Transform each MGP $\hat{\mathbf{z}}^{(i)}$ to bicycle coordinate system.
4: Calculate measurement to MGP distances as $|\mathbf{z}_{\mathsf{x}}^{(j)} - \hat{\mathbf{z}}_{\mathsf{x}}^{(i)}|$.
5: Associate each measurement to the closest MGP.
6: **Output:** Associations $\{j\ ,\ \rho(j)\}$.

Measurement transformation function
1: **Input:** Cell $W = \left\{\mathbf{z}^{(j)}\right\}$, estimate $\hat{\mathbf{x}}$
2: Transform to bicycle coordinate system: $\mathbf{z}^{(j)} \leftarrow R(\hat{\phi})\left(\mathbf{z}^{(j)} - [\hat{\mathsf{x}}\ \hat{\mathsf{y}}]^{\text{T}}\right),\ \forall j$, where $R(\phi)$ is a $2D$ rotation matrix.
3: Shift x-coordinates: $\mathbf{z}_{\mathsf{x}}^{(j)} \leftarrow \mathbf{z}_{\mathsf{x}}^{(j)} - \min_j \mathbf{z}_{\mathsf{x}}^{(j)},\ \forall j$
4: Rescale x-coordinates: $\mathbf{z}_{\mathsf{x}}^{(j)} \leftarrow \ell\mathbf{z}_{\mathsf{x}}^{(j)}/\max_j \mathbf{z}_{\mathsf{x}}^{(j)},\ \forall j$
5: Shift x-coordinates: $\mathbf{z}_{\mathsf{x}}^{(j)} \leftarrow \mathbf{z}_{\mathsf{x}}^{(j)} - \ell/2,\ \forall j$
6: **Output:** Transformed cell

Thus, for the point measurement model the predicted measurement, Jacobian and covariance, cf. Section III-B, are $\hat{\mathbf{z}}_W^{(j)}(o) = \mathbf{H}_W m_{k|k-1}^{(j)}(o)$, $H_k^{(j)}(o) = \mathbf{H}_W$ and $R_k(o) = \sigma_P^2\mathbf{I}_{2|W|}$, respectively.

2) Line measurement model: The line measurement model corresponds to when the bicycle's orientation is such that either the left or right side of the bicycle can bee seen. This corresponds to $\cos(\beta) \approx 0$ in Fig. 2. In this case the measurements in the cell are spread along the entire length of the bicycle: from the rear wheel to the front wheel. In previous work [3]–[5] where the extended target has been model as stick shaped, the measurements have been assumed to be spread uniformly along the length of the stick. For example each measurement can be seen as a uniformly distributed random sample along the stick, with added Gaussian noise,

$$p(W|\mathbf{x}) = \prod_{\mathbf{z}\in W} p(\mathbf{z}|\mathbf{y})\, p(\mathbf{y}|\mathbf{x}) \tag{28a}$$

$$= \prod_{\mathbf{z}\in W}\mathcal{N}(\mathbf{z}; \mathbf{y}, R)\,\mathcal{U}(\mathbf{y}; \mathbf{x}). \tag{28b}$$

Here the set of measurements is instead modeled as being caused by a set of measurement generating points (MGP) $\hat{\mathbf{z}}^{(i)}(\mathbf{x})$ located along the stick shape. Given a predicted target kinematics estimate $\hat{\mathbf{x}}_{k|k-1}$, computing the predicted location of these MGPs is easy using line intersection. A set of measurement to MGP associations $\{j\ ,\ \rho(j)\}$ are obtained using the method outlined in Table II. Note that multiple measurements can be associated to the same MGP, and in a sense each MGP can be interpreted as an extended target without a shape model. The likelihood is

$$p(W|\mathbf{x}, o=3,4) = \prod_{j=1}^{|W|}\mathcal{N}\left(\mathbf{z}_k^{(j)}\,;\,\hat{\mathbf{z}}^{(\rho(j))}(\mathbf{x}), \sigma_L^2 I_2\right) \tag{29a}$$

$$= \mathcal{N}\left(\mathbf{z}_W\,;\,\hat{\mathbf{z}}_W(\mathbf{x}), \sigma_L^2 I_{2|W|}\right), \tag{29b}$$

where $\hat{\mathbf{z}}_W(\mathbf{x})$ is a vertical vectorial concatenation of the MGPs in the order specified by the association. For the line measurement model the predicted measurement and covariance are $\hat{\mathbf{z}}_W\left(m_{k|k-1}^{(j)}(o)\right)$ and $R_k(o) = \sigma_L^2 I_{2|W|}$, respectively. The Jacobian $H_k^{(j)}(o)$ can be computed analytically, however the tedious details are omitted.

V. Results

The implemented MM-ET-PHD filter has been evaluated using several different data sets that have been collected at the Linköping University campus over the course of two years. In this section we present results from three of the data sets: two with a single target in Section V-A, and one with two targets in Section V-B. The results obtained for these three data sets are representative of the overall performance of the MM-ET-PHD filter, and also highlight interesting aspects of the estimation. The measurements were acquired using a SICK LMS laser range sensor that measures range every 0.5° over a 180° surveillance area. The sensor was elevated approximately $40\,\mathrm{cm}$ above the ground, which corresponds to approximately the same height as distance sensors usually are mounted in standard passenger cars. The measurements were converted to (x, y) measurements using a polar to Cartesian transformation, and to remove measurements caused by the stationary background only ranges shorter than $r_{\max}\mathrm{m}$ were used. Because the data sets were collected at different occasions different values for $r_{\max}$ between $10\mathrm{m}$ and $15\mathrm{m}$ had to be used.

In the MM-ET-PHD implementation the constant length of the bicycles was set to $\ell = 1.75$. The motion model parameters were set to $P_S = 0.99$, $P_{\text{same}} = 0.90$, $P_{\min} = 0.01$, $\sigma_v = 0.2$, $\sigma_\omega = 0.2$, and the measurement model parameters were set to $P_D = 0.99$, $\gamma = 20$, $\lambda_k c_k(\mathbf{z}_k) = 2\pi^{-1} r_{\max}^{-2}$, $\sigma_P = 0.1$, $\sigma_L = 0.075$. For pruning a threshold $\tau = 10^{-3}$ was used, for merging a threshold $U = 1$ was used.

Similarly to [24], [25] the birth PHD contains Gaussian components spread uniformly along the edge of the surveillance area. Because of the non-linearity of the motion and measurement models the birth PHD must not contain to few Gaussian components. In the implementation, for each mode, there were 20 components along the semi-circular edge, and 14 components along the x-axis. The positions of the birth components were chosen such that the front end of the stick estimate is just inside the surveillance area.

There is no ground truth available for the data sets and thus standard performance measures like the OSPA or the RMSE cannot be used, instead the results are evaluated using visual inspection of the tracking results. The proposed method to use multiple measurement models is compared to using only the single models, i.e. either only the point model or only the line model.

A. Single Target

In the two single target data sets the target transitions from CV motion to a CT maneuver at a position in the state space that means that it also transitions from the L mode to the P mode. Assume that the sensor is mounted in the grille of a standard passenger car driving straight on a road. Then the first experiment in Fig. 3 corresponds to a bike coming from the right, turning abruptly and then moving towards the car. The second experiment in Fig. 4 corresponds to a bike coming from the right, turning away from the car and then biking in the same direction as the car. The data is shown in Fig. 3a and 4a, and tracking results using the proposed MM-ET-PHD filter are shown in Fig. 3b and 4b. Overall the measurement modes of the extracted targets correspond to expectations; the point measurement mode is typically used when the bicycle is lined up with the bearing between the sensor and the bicycle's center point.

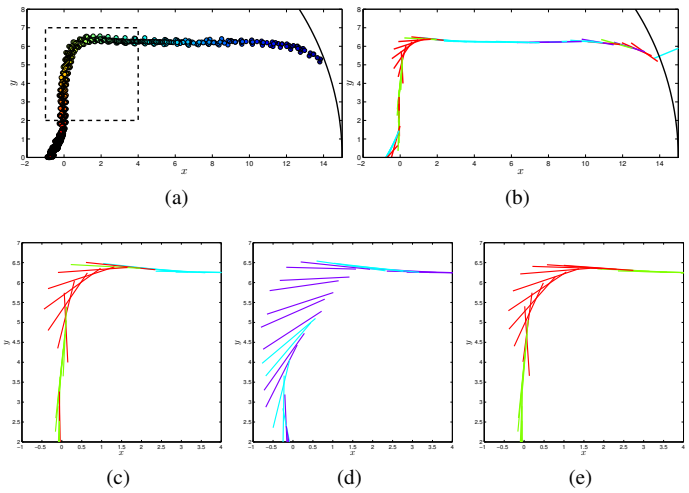

Fig. 3. Bicycle tracking results, the estimates are color coded according to the different modes: red for CTP, green for CVP, cyan for CTL and purple for CVL. (a) Measurements. (b) Tracking results using multiple measurement models. (c), (d) and (e): Comparison of tracking results during maneuver for multiple measurements models, the line measurement model, and point measurement model, respectively.

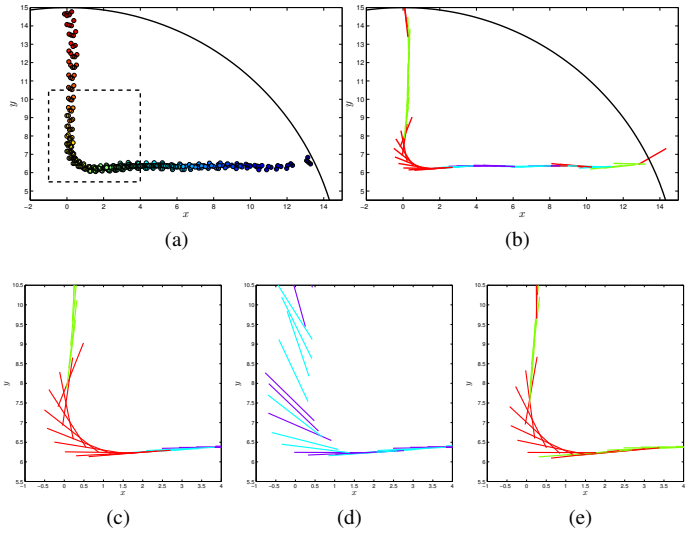

Fig. 4. Bicycle tracking results, the estimates are color coded according to the different modes: red for CTP, green for CVP, cyan for CTL and purple for CVL. (a) Measurements. (b) Tracking results using multiple measurement models. (c), (d) and (e): Comparison of tracking results during maneuver for multiple measurements models, the line measurement model, and point measurement model, respectively.

Comparisons of the MM results and results using the single measurement models are given in Fig. 3c to 3e, and Fig. 4c to 4e. It is evident that when using only the line measurement model, the heading is not estimated correctly during the maneuver. Note that since the MM chooses the point mode during the turn, there is no obvious difference between the MM and the point model during the maneuver.

B. Multiple Targets

In the multiple target data set two bicycles move around inside the surveillance area, and there are eight different occasions at which a target either enters or exits the surveillance area. The data is shown in Fig. 5a, and tracking results using the proposed MM-ET-PHD filter are shown in Fig. 5b. As in the single target experiments there is a reasonable overall correspondence between the extracted targets' modes and what can be expected from a target given the kinematic state. The L measurement mode is much more common than the P mode, because in this data the bicycles rarely move straight towards/away from the sensor.

In Fig. 5c a subset of the data is shown, and a comparison for this data between the result of the MM and the results using the single measurement models is given in Fig. 5d to 5f. When the target enters the surveillance area, the heading estimate has a larger error when only the P measurement model is used. There are two additional time steps for which the P model heading estimates are incorrect, around $(x,\ y) = (1,\ 2.5)$ in Fig. 5f. For remaining time steps the P model gives results comparable to the MM results. The problems for the P model are related to the fact that the heading is not observable from a single set of measurements, but has to be estimated using a time sequence of measurement sets. If the sensor is mounted on a moving platform, e.g. a car driving through urban traffic, correct initial estimates are of increasing importance for the understanding of a multiple extended target scene.

C. Summary

The presented results show that using only the line measurement model does not give sufficiently good results in all situations. Using only the point measurement model works in most cases, however when the measurements are "line-shaped", the line measurement model (typically) gives a better heading estimate, especially when the target enters the surveillance area. These observations are pursuant to the statements about the three modeling levels introduced in Section I. The amount of information present in the measurements is crucial for the observability of the target state, especially the extension parameters. The point measurement model is applicable in all appearance modes and will most often produce a reasonable estimate of the target's position and heading. However, if the measurements are line-shaped, and hence the stick parameters are observable, this extra information can improve the estimates of other states too. On the contrary, if the stick extension is not observable and only the line measurement model is used the estimates of other state variables, such as the heading, will also suffer.

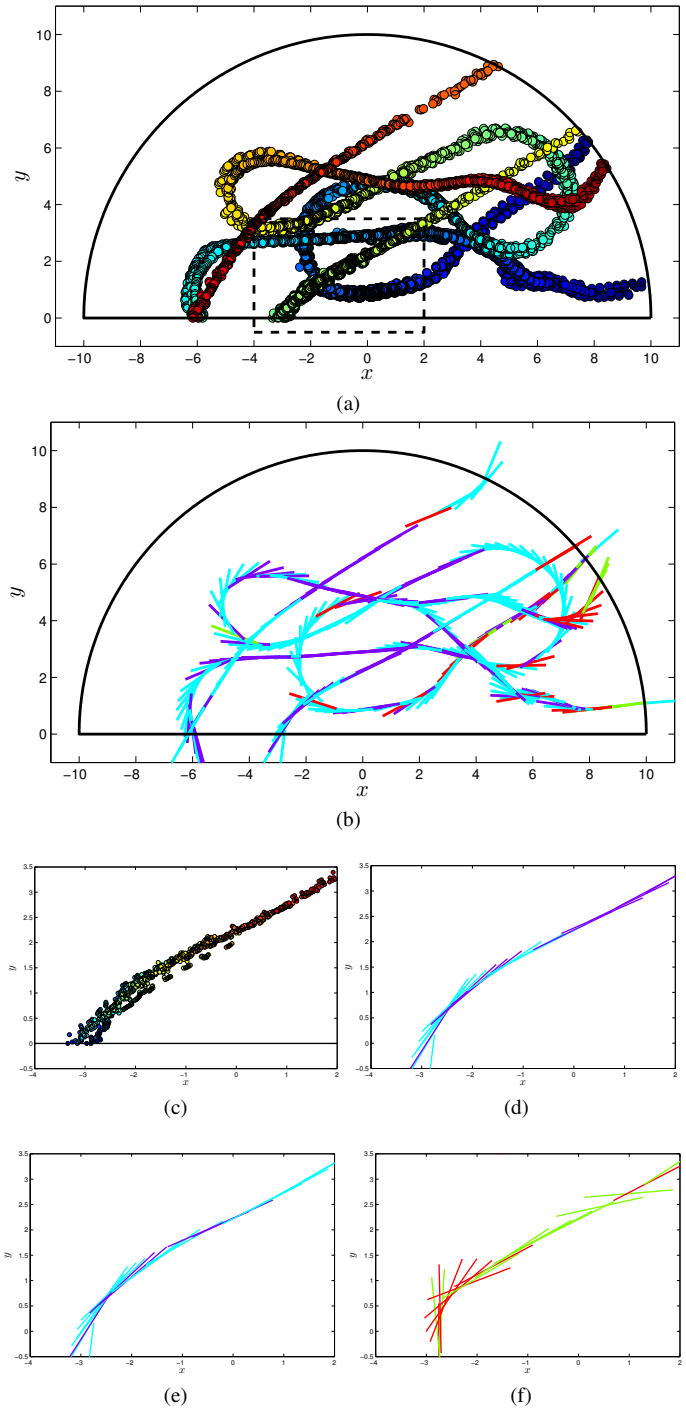

Fig. 5. Bicycle tracking results, the estimates are color coded according to the different modes: red for CTP, green for CVP, cyan for CTL and purple for CVL. (a) Measurements. (b) Tracking results using multiple measurement models. (d), (e) and (f): Comparison of tracking results during maneuver for multiple measurements models, the line measurement model, and point measurement model, respectively.

VI. Conclusions and Future Work

The use of multiple measurement models to track extended targets whose appearances alter abruptly is studied in this publication. The appearance of extended target measurements can change with the sensor to target geometry. When using different measurement models, the one which fits best to the measurement data should be used because the observability of the state variables is maximized in that way. If the target's extension parameters are observable in the data, the extension should be estimated. However, if the extension parameters are not observable a simplified measurement model should be used to update only the observable states.

In this work the multiple measurement model has been exemplified using laser data generated from bicycles maneuvering in front of the sensor. Under an assumed constant length two measurement models are studied, one stick model and one

point model. In future work estimation of the length of the bicycles will be added. In this case the appearance modes are of even higher importance, since the length is only observable from line measurements, and not from point measurements. A comparison to other measurement models for stick shaped extended targets would be interesting.

REFERENCES

[1] Y. Bar-Shalom and T. E. Fortmann, *Tracking and data association*, ser. Mathematics in Science and Engineering. San Diego, CA, USA: Academic Press Professional, Inc., 1987, vol. 179.

[2] K. Granström, C. Lundquist, and U. Orguner, "Tracking Rectangular and Elliptical Extended Targets Using Laser Measurements," in *Proceedings of the International Conference on Information Fusion*, Chicago, IL, USA, Jul. 2011, pp. 592–599.

[3] K. Gilholm, S. Godsill, S. Maskell, and D. Salmond, "Poisson models for extended target and group tracking," in *Proceedings of Signal and Data Processing of Small Targets*, vol. 5913. San Diego, CA, USA: SPIE, Aug. 2005, pp. 230–241.

[4] K. Gilholm and D. Salmond, "Spatial distribution model for tracking extended objects," *IEE Proceedings of Radar, Sonar and Navigation*, vol. 152, no. 5, pp. 364–371, Oct. 2005.

[5] M. Baum, F. Faion, and U. D. Hanebeck, "Modeling the Target Extent with Multiplicative Noise," in *Proceedings of the International Conference on Information Fusion*, Singapore, Jul. 2012, pp. 2406–2412.

[6] Y. Boers, H. Driessen, J. Torstensson, M. Trieb, R. Karlsson, and F. Gustafsson, "A track before detect algorithm for tracking extended targets," *IEE Proceedings Radar, Sonar and Navigation*, vol. 153, no. 4, pp. 345–351, Aug. 2006.

[7] N. Petrov, L. Mihaylova, A. Gning, and D. Angelova, "A novel sequential monte carlo approach for extended object tracking based on border parametrisation," in *Proceedings of the International Conference on Information Fusion*, Chicago, IL, USA, Jul. 2011, pp. 306–313.

[8] J. W. Koch, "Bayesian approach to extended object and cluster tracking using random matrices," *IEEE Transactions on Aerospace and Electronic Systems*, vol. 44, no. 3, pp. 1042–1059, Jul. 2008.

[9] M. Baum, B. Noack, and U. D. Hanebeck, "Extended Object and Group Tracking with Elliptic Random Hypersurface Models," in *Proceedings of the International Conference on Information Fusion*, Edinburgh, UK, Jul. 2010.

[10] H. Zhu, C. Han, and C. Li, "An extended target tracking method with random finite set observations," in *Proceedings of the International Conference on Information Fusion*, Chicago, IL, USA, Jul. 2011, pp. 73–78.

[11] S. Reuter and K. Dietmayer, "Pedestrian tracking using random finite sets," in *Proceedings of the International Conference on Information Fusion*, Chicago, IL, USA, Jul. 2011, pp. 1101–1108.

[12] J. Degerman, J. Wintenby, and D. Svensson, "Extended target tracking using principal components," in *Proceedings of the International Conference on Information Fusion*, Chicago, IL, USA, Jul. 2011, pp. 330–337.

[13] J. Lan and X. Rong Li, "Tracking of extended object or target group using random matrix – part I: New model and approach," in *Proceedings of the International Conference on Information Fusion*, Singapore, Jul. 2012, pp. 2177–2184.

[14] S. Reuter, B. Wilking, and K. Dietmayer, "Methods to model the motion of extended objects in multi-object Bayes filters," in *Proceedings of the International Conference on Information Fusion*, Singapore, Jul. 2012, pp. 527–534.

[15] C. Lundquist, K. Granström, and U. Orguner, "Estimating the Shape of Targets with a PHD Filter," in *Proceedings of the International Conference on Information Fusion*, Chicago, IL, USA, Jul. 2011, pp. 49–56.

[16] M. Baum and U. D. Hanebeck, "Shape Tracking of Extended Objects and Group Targets with Star-Convex RHMs," in *Proceedings of the International Conference on Information Fusion*, Chicago, IL, USA, Jul. 2011, pp. 338–345.

[17] H. Blom and Y. Bar-Shalom, "The interacting multiple model algorithm for systems with Markovian switching coefficients," *IEEE Transactions on Automatic Control*, vol. 33, no. 8, pp. 780–783, aug 1988.

[18] M. Feldmann, D. Fränken, and J. W. Koch, "Tracking of extended objects and group targets using random matrices," *IEEE Transactions on Signal Processing*, vol. 59, no. 4, pp. 1409–1420, Apr. 2011.

[19] R. Mahler, *Statistical Multisource-Multitarget Information Fusion*. Norwood, MA, USA: Artech House, 2007.

[20] ——, "Multitarget Bayes filtering via first-order multi target moments," *IEEE Transactions on Aerospace and Electronic Systems*, vol. 39, no. 4, pp. 1152–1178, Oct. 2003.

[21] B.-N. Vo and W.-K. Ma, "The Gaussian mixture probability hypothesis density filter," *IEEE Transactions on Signal Processing*, vol. 54, no. 11, pp. 4091–4104, Nov. 2006.

[22] R. Mahler, "PHD filters for nonstandard targets, I: Extended targets," in *Proceedings of the International Conference on Information Fusion*, Seattle, WA, USA, Jul. 2009, pp. 915–921.

[23] K. Granström, C. Lundquist, and U. Orguner, "A Gaussian mixture PHD filter for extended target tracking," in *Proceedings of the International Conference on Information Fusion*, Edinburgh, UK, Jul. 2010.

[24] ——, "Extended Target Tracking using a Gaussian Mixture PHD filter," *IEEE Transactions on Aerospace and Electronic Systems*, vol. 48, no. 4, pp. 3268–3286, Oct. 2012.

[25] K. Granström and U. Orguner, "A PHD filter for tracking multiple extended targets using random matrices," *IEEE Transactions on Signal Processing*, vol. 60, no. 11, pp. 5657–5671, Nov. 2012.

[26] R. Mahler, "On Multitarget Jump-Markov Filters," in *Proceedings of the International Conference on Information Fusion*, Singapore, Jul. 2012, pp. 149–156.

[27] S. Pasha, B.-N. Vo, H. Tuan, and W.-K. Ma, "A Gaussian mixture PHD filter for jump Markov system models," *IEEE Transactions on Aerospace and Electronic Systems*, vol. 45, no. 3, pp. 919–936, Jul. 2009.

[28] K. Granström and U. Orguner, "On Spawning and Combination of Extended/Group Targets Modeled with Random Matrices," *IEEE Transactions on Signal Processing*, vol. 61, no. 3, pp. 678–692, Feb. 2013.

[29] Y. Bar-Shalom, P. K. Willett, and X. Tian, *Tracking and data fusion, a handbook of algorithms*. YBS, 2011.

[30] X. Rong Li and V. Jilkov, "Survey of maneuvering target tracking: Part I. Dynamic models," *IEEE Transactions on Aerospace and Electronic Systems*, vol. 39, no. 4, pp. 1333–1364, Oct. 2003.

[31] K. Granström and U. Orguner, "On the Reduction of Gaussian inverse Wishart mixtures," in *Proceedings of the International Conference on Information Fusion*, Singapore, Jul. 2012, pp. 2162–2169.

[32] T. Yuan, Y. Bar-Shalom, P. Willett, E. Mozeson, S. Pollak, and D. Hardiman, "A multiple IMM estimation approach with unbiased mixing for thrusting projectiles," *IEEE Transactions on Aerospace and Electronic Systems*, vol. 48, no. 4, pp. 3250–3267, Oct.